Chapter 2
Nano Architectures in Silicon Photovoltaics

Nazir P. Kherani

Abstract A historical trace of key developments in the science and engineering of photovoltaics introduces the reader to this important field of energy generation. An overview of photovoltaics and allied photonic architectures is presented including a synopsis of the relevant physics. A selected illustrative review of recent research results on the integration of wave-optic coupling nanostructures in silicon photovoltaics is given with an emphasis on the use of photonic crystal constructs. The chapter closes pondering the arc of development in silicon photovoltaics—the main stay of present day solar photovoltaics.

2.1 Introduction

Maxwell's equations, presented in 1864 to the Royal Society of London [1], remarkably remain to this day an adequate and elegant description of the underlying electromagnetic field for essentially all atomic and condensed matter phenomena [2]—notwithstanding the superseding comprehensive description of light–matter interactions provided by quantum electrodynamics [3, 4]. Within this framework, the physical structure or architecture[1] of systems have yielded extraordinary physical effects. Through the integrative effect of electromagnetic interactions in

[1] Structure is the arrangement and relationship among the constitutive parts of a given system; hence architecture is the physical structure of a system.

N. P. Kherani (✉)
Department of Electrical and Computer Engineering, University of Toronto,
10 King's College Road, Toronto, ON M5S 3G4, Canada
e-mail: nazir.kherani@gmail.com

N. P. Kherani
Department of Materials Science and Engineering, University of Toronto,
184 College Street, Toronto, ON M5S 3E4, Canada
e-mail: Kherani@ecf.utoronto.ca

J. Singh and R. T. Williams (eds.), *Excitonic and Photonic Processes in Materials*,
Springer Series in Materials Science 203, DOI: 10.1007/978-981-287-131-2_2,

atomic or condensed matter systems, novel classes of materials have been produced which include metamaterials [5–7], photonic crystals [8–12] and plasmonic materials [13–15]. Further, the advent of advanced materials synthesis capabilities, particularly at the micrometer and nanometer length scales [16, 17], and the ready accessibility to powerful numerical computational tools, has ushered a cornucopia of research examining the practical applicability of these basic phenomena to information and communication technologies, medical diagnostics and therapies, and energy systems to name a few. The photovoltaic effect, generation of an electric potential between two electrodes upon exposure of the system to light, first observed by Edmond Becquerel and reported in 1839 [18] is the basis of direct conversion of light energy into electricity. Following a number of research advances in the intervening 100 plus years, in 1954 the first crystalline silicon photovoltaic device was developed at Bell Laboratories with an AM1.5[2] one sun photovoltaic energy conversion efficiency of 6 % [19]. This first silicon solar cell, a photodiode that operates in a passive externally-unbiased mode transducing light energy in to electrical energy, heralded a new technologically-viable globally-accessible renewable energy industry—solar photovoltaics or simply solar electricity. The enormous potential of this renewable energy source is self-evident in the solar irradiance map of the world, shown in Fig. 2.1.

Over the last six decades, crystalline silicon solar cells have experienced extensive scientific and technological advances that have led to record AM1.5 photovoltaic conversion efficiencies of 25 % for 400 micron thick silicon in the laboratory [20], recently to 24 %+ conversion efficiencies for less than 200 micron thick back-contact siliconsolar cells in industrial production,[3] and more recently 24.7 % for less than 100 micron thick low-temperature synthesized silicon solar cells [21] and even more recently 25.6 % for similar back-contact solar cells.[4] Concurrently, several other competing solar materials have developed into complementary commercial photovoltaic systems which include thin film cadmium telluride (CdTe), thin film copper indium gallium diselenide (CIGS), copper zinc tin sulphide (CZTS), thin film amorphous-microcrystalline silicon, and III–V crystalline semiconductor based concentrated photovoltaics [22–24].

Recently the field of photovoltaics has attracted much research attention spurred by a range of socioeconomic and environmental concerns and the resolve of a variety of stake holders to make solar electricity an economically inevitable reality. This has led to an exploration of a plethora of novel material systems for photovoltaic applications, some of which include dye sensitized solar cells [25–28], organic photovoltaics [29, 30], quantum dot solar cells [31, 32], and perovskites [33, 34], as well

[2] AM1.5 represents a standard solar spectrum with an integrated irradiance of 1,000 Wm^{-2} [ref], which corresponds on average to the irradiance level at mid-latitudes (corresponding to a solar zenith angle of $Z = 48.2°$)—where the rays of the sun traverse an air mass of 1.5 times the thickness of the atmosphere at the equator, at the zenith.

[3] http://www.renewableenergyworld.com/rea/news/article/2010/06/sunpower-sets-solar-cell-efficiency-record-at-24-2.

[4] http://www.panasonic.co.jp/corp/news/official.data/data.dir/2014/04/en140410-4/en140410-4.html.

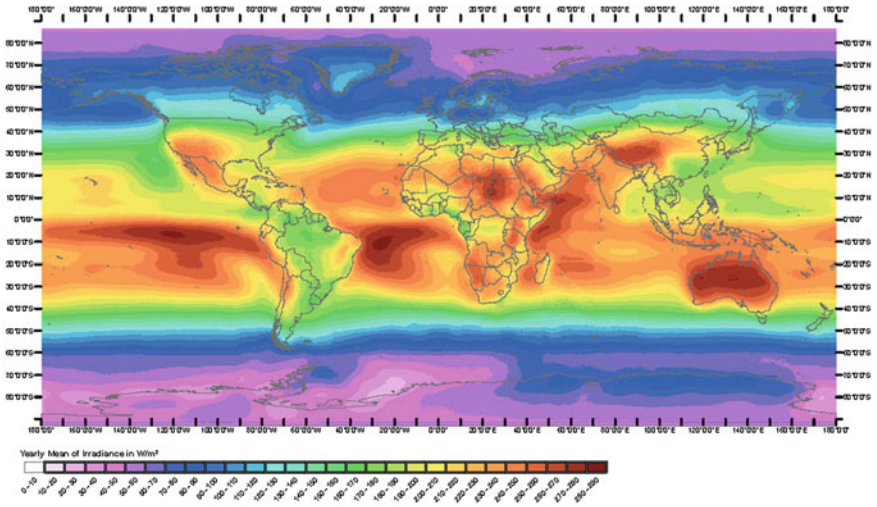

Fig. 2.1 Average solar irradiance map of the world illustrating the enormity of the distributed solar resource and that the variability/uniformity in the irradiance among most regions of the world lies within a factor of three. Copyright Mines Paristech/Armines 2006

as a further investigation of the incumbent photovoltaic material system of silicon. In this quest, the architecture of photovoltaic devices has played an increasingly important role, effecting changes in the optical and electrical properties of the systems. For example, quantum confinement effects are being considered in the pursuit of complete utilization of the solar spectrum and have led to the study of a range of quantum dot material systems including silicon [35–37]. In other cases, simply complete optical absorption of the supra-bandgap part of the solar spectrum have led to the study of a range of photonic constructs to effect the desired optical coupling [38, 39]. And yet in other instances, the need to effectively integrate new photonic constructs while addressing the device's electrical requirements of charge transport have been pursued [40–45].

With the advent of nanostructured material synthesis, the prospect of realizing novel optical and electrical effects in the entire gamut of solar materials including silicon has invigorated fundamental and applied research to new heights. In silicon, the expectation is that this terrestrially abundant, environmentally compatible, and industrially established material can be newly engineered to yield high optical to electrical conversion efficiency while requiring a minimal quantity of the material, and thus resulting in a ubiquitous energy converter at the lowest cost per watt [46, 47]. On the immediate horizon, the objectives are to explore existing crystalline silicon and thin film silicon platforms while in the longer term novel approaches such as nano-wire, nano-crystalline/particle and other nano-structures of silicon are being contemplated.

For crystalline silicon, the arc of progress is towards ultra-thin silicon which in the limit exacts light trapping at optical and infrared wavelengths, while for thin film amorphous-microcrystalline silicon the challenge is to not only harvest the light but to spectrally mold its flow in tandem device structures. Further, both platforms demand broad band absorption over broad angular incidence considering the outlook of stationary solar panels generating more energy without the need for solar trackers. Nanostructuring of dielectrics and semiconductors offering wave-optic coupling, light localization and light trapping indicate effective means of mitigating optical reflection at the incident interface, enhancing the path length of light within the absorber, and effectively back-reflecting the light at the far interface. The integration of such nano-architectures in silicon promises a path to the next generation of economically inescapable subsidy-free silicon photovoltaic solar cells.

In this chapter, we present an overview of photovoltaics and allied photonic architectures with an emphasis on approaches to enhance optical absorption, a synopsis of the physics pertaining to photovoltaics and photonic structures, and then provide a selected review of recent research results advancing the integration of wave-optic coupling in silicon photovoltaics and in particular highlighting the use of photonic crystal constructs.

2.2 Photovoltaics and Photonic Architectures: A Historical Perspective

2.2.1 Photovoltaics

In 1839 Edmond Becquerel while carrying out an electrolytic experiment observed an electrical response in the external circuit upon exposure of silver coated platinum electrodes to light, thus marking the beginning of the science of photovoltaics. In 1873 Willoughby Smith discovered the photoconductivity of selenium [48] which established the basis for the demonstration of the solid state photovoltaic effect by William Adams and Richard Day several years later in 1876 [49, 50]. Adams and Day, having made platinum contacts on a selenium rod, observed a change in the electrical characteristics of selenium upon light exposure and thus paved the way for the demonstration of the first solid state photocell.

In 1883 Charles Fritts fabricated the first solar cell by melting a 30 μm thin sheet of selenium onto an iron substrate followed by pressing down a 5 nm thin transparent leaf of gold on selenium, hence marking the beginning of the technology of photovoltaics [51]. Of the range of materials examined Fritts found that the photovoltaic action was most significant with brass, zinc and iron, reflective of the formation of different Schottky devices. The Schottky photovoltaic device was 30 cm^2 in area and operated at a conversion efficiency of approximately 1 % much lower than Fritts' expectations and his underlying hope of competing with Thomas Edison's coal-fired power plants.

In 1954 the celebrated report by Chapin, Pearson and Fuller of a silicon photovoltaic cell with a conversion efficiency of 6 % marked the beginning of the modern era of the science and technology of photovoltaics [19]. This extraordinary achievement was due to earlier research principally motivated by the development of silicon electronics. Notably, the development of point-contact diodes, also known as cat's whisker diodes, in the early part of the twentieth century led to the replacement of thermionic valves in most applications. These diodes which required the pressing of metal wires against polycrystalline silicon exhibited significant variability in performance owing to the substantial presence of impurities which resulted in so called "hot spots" in silicon. Russel Ohl at Bell Laboratories surmised the importance of growing purer silicon and thus led a series of experiments synthesizing the purest silicon ingots possible. These experiments led to the first observation of a photovoltage of approximately 0.5 V upon illuminating the diode with a flashlight. It is interesting to note that these early silicon devices were due to a fortuitous distribution of boron rich and phosphorus rich impurity regions that gave rise to contiguous *p*-type and *n*-type regions, respectively, during the growth of the silicon ingot. The first silicon photovoltaic devices were synthesized by slicing sections of the ingot that contained adjoining *p*-doped and *n*-doped regions followed by metallization of the doped surfaces. These first *pn* barrier or *pn* junction silicon devices, reported by Ohl in 1941, exhibited photovoltaic conversion efficiencies of a fraction of a percent [52]. Excerpts and figures taken from Russel S. Ohl's 1941 patent are shown in Fig. 2.2. With the recognition that controlled synthesis was critical in advancing device performance, major developments in the synthesis of single crystal silicon using the Czochlralski process and thermal diffusion of dopant impurities into the surface of silicon led to the remarkable performance of the first 6 % silicon solar cell.

These developments in the 1950s engendered enormous interest and ushered an expectation of remarkable progress in future silicon devices. Motivated by space applications, silicon solar cells with efficiencies of approximately 15 % under one sun conditions were developed by the 1960s [53]. Further, spurred by the oil embargo of the seventies, silicon photovoltaics experienced yet another surge of development leading to record one sun efficiency of 25 % [20] and concentrated[5] 100 suns efficiency of almost 28 % [54]. The principal developments making this possible include a series of materials and device configurational advances that have made complete optical absorption and photogeneration possible followed by effective separation of the photocarriers to yield maximal potential, current density and fill factor. At the materials level, the production of high quality single- and multi-crystalline silicon, surface preconditioning, and control over the diffusion processes have been key. Further, the importance of front and rear surface passivation through the reduction of interfacial defect densities (chemical passivation) and trapped surface charge (field passivation) have played a marked role in enhancing the open circuit potential of the devices as well as the current density; in this context, the passivation proper-

[5] Concentrated photovoltaics, attained using various optical field enhancement techniques, invariably yields a higher performance cell principally attributed to the increase in the open circuit voltage of the cell.

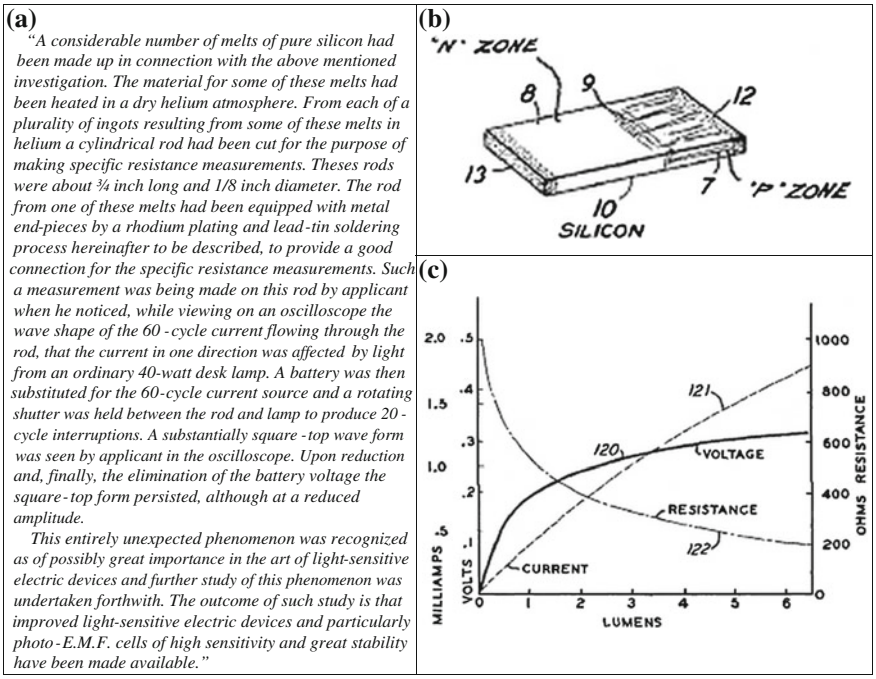

Fig. 2.2 Excerpts and figures from Russel S. Ohl's patent on *Light-Sensitive Electric Device* filed in 1941. **a** Excerpt recounting the manner of the discovery. **b** An illustration of the silicon *pn* junction highlighting the *p* (*7*) and *n* (*8*) regions, as well as the barrier region (*9*) which as described by Ohl is "apparently the seat of the photo-E.M.F. effect", and the contacts (*12* and *13*). **c** A plot of the cell's current, voltage and resistance as a function of the illumination [52]

ties of thermal oxide have been superlative. Incorporation of light trapping features have been principally addressed through patterning/texturing of front (light-facing) and rear surfaces, antireflective layers and back reflection coatings. Minimization of ohmic losses through reduction of contact and line (grid and bus bar) resistances, work function terracing, and reduction of shadowing losses have been key in the attainment of large area crystalline silicon solar cells. Today, the crystalline silicon photovoltaics industry has matured to a level where commercial solar cells are routinely produced at efficiencies typically ranging from 17 to 20+ % using silicon wafers as thin as 150–180 μm. Further, crystalline silicon photovoltaics over the last several decades has commanded 80–90 % of the market share and accordingly has contributed towards an estimated cumulative installed global PV capacity of 100 GWp[6] as of 2012 [55].

[6] GWp represents gigawatts of electricity generation under peak 1 sun (nominally 1,000 W/m^2) illumination. Photovoltaic generating capacity factors can vary from approximately 11–23 % corresponding to moderate to very high insolation (solar irradiation) sites.

Concurrent to the above described progress in crystalline silicon photovoltaics, a number of alternative approaches have been proposed [56–58]. We highlight two significant concepts the development of which have led to successful production and deployment in the field. The first is the archetype of thin film photovoltaics using silicon. In 1975 Spear and LeComber reported the successful enhancement in conductivity of hydrogenated amorphous silicon (aSi:H) using diborane and phosphine as precursor impurity doping gases in a silane plasma [59]. In 1976 David Carlson and Christopher Wronski successfully reported a thin film amorphous silicon solar cell with a conversion efficiency of 2.4 % [60]. Following several years of research the importance of hydrogen passivation of gap states in amorphous silicon was recognized as essential to the attainment of superior electronic properties. This advance led to single and multijunction hydrogenated amorphous silicon solar cells with stabilized efficiencies exceeding 10 % [61]. Further, the successful plasma-based growth of microcrystalline or nanocrystalline silicon thin films [62], wherein the films contain a large fraction of crystallites of silicon in a backdrop of hydrogenated amorphous silicon, led to the development of the all-silicon dual junction micromorph[7] solar cell—a cell concept that effectively dispenses with the use of germanium alloying in hydrogenated amorphous silicon used to narrow the bandgap of the absorber. Stabilized solar cell efficiencies of approximately 12–13 % for the micromorph cell have been demonstrated wherein the role of material quality, including film thickness and stability considerations, and light trapping features are evidently unavoidable characteristics [63, 64].

The second is a paradigm shift in the synthesis of crystalline silicon solar cells. The advent of amorphous silicon–crystalline silicon heterojunction has brought about the successful synthesis of record efficiency crystalline silicon cells fabricated at temperatures of less than 250 °C. In this approach nanometer thin films of intrinsic and doped hydrogenated amorphous silicon are deposited directly on silicon to attain high quality interfacial passivation and junction formation, respectively. The first silicon heterojunction cells reported by Tanaka et al. reported conversion efficiency exceeding 18 % using intrinsic a-Si:H [65]; more recently, an efficiency of 24.7 % using 98 μm thick c-Si has been reported by Panasonic. A host of similar heterojunction cell concepts have been investigated and reported by a number of other researchers [66]. Concurrently, much research has been underway examining alternative passivation materials, such as hydrogenated amorphous carbon, to overcome the unavoidable parasitic optical absorption losses of a-Si:H. Within this framework various cell concepts have been advanced including complete low temperature synthesis of back contact silicon solar cells [67, 68]. Further, alternative passivation techniques have been explored such as hydrogen plasma treatment of the amorphous silicon layer, the use of atomic layer deposited materials and various bilayer structures including the use offacile grown native oxideson crystalline silicon [69–72]. Moreover, the heterojunction paradigm is deemed to be a particularly viable approach to the synthesis of economic high-efficiency ultra-thin silicon solar cells.

[7] Consisting of a hydrogenated amorphous silicon *pin* solar cell ($E_g \sim 1.7$ eV) in tandem with an underlying microcrystalline silicon *pin* cell ($E_g \sim 1.1$ eV).

The foregoing synopsis illustrates the remarkable journey of silicon photovoltaics which has undoubtedly benefitted from the well-established silicon microelectronic industry. Notwithstanding the progress, silicon photovoltaics continues to be challenged economically and as a result much research has been underway to investigate new incremental enhancements that can be readily integrated in existing silicon solar cell concepts as well as explore novel approaches that may potentially leapfrog existing technologies. It is worth noting that while further economic gains can be made at the silicon cell level, parallel efforts in the effective vertical integration from cell to panel to deployment in the field is essential so as to ultimately break the economic barrier. Within this framework, there is a prevailing view that advances at the cell level along with effective vertical integration can make this possible. Accordingly, much attention has also been given to effectively harvest solar photons using advanced photonic constructs. We now provide a selected overview of light-matter interactions and the subsequent development of photonic structures for effective control over the flow of light from a photovoltaic perspective.

2.2.1.1 Photonic Architectures

Historically the science of optics originates with Euclid around 300 BC [73] and the subsequent Alexandrians Heron and Ptolemy [74] who followed him, providing the first narrative on the laws of reflection and indicating observations of optical aberration—notwithstanding archaeological discovery of the Nimrud rock crystal lens that suggests optical acumen may date as far back as 750 BC among the Assyrians. Almost 2 millennia later in 1621 Snell presented the law of refraction and in 1657 Fermat outlined the principle of least time that defined the path taken by a ray of light, a principle consistent with Snell's law[8] [75]. Fresnel whose work spanned from 1816 to 1821 helped definitively establish the validity of the wave theory of light, his crowning work showing that light is a transverse wave. Today, the Fresnel equations provide a detailed description of the reflection and transmission or refraction of light impinging a planar interface between media of different refractive indices—clearly accounting for the polarization of light. Optical effects such as complete transmission of *p*-polarized light at the Brewster angle and total internal reflection at angles exceeding the critical angle for light traversing from larger index to smaller index media emerge clearly from the Fresnel equations. Further, the Fresnel equations are the basis of studying a number of interference phenomena which include iridescence, antireflection coatings, optical filters, and interferometers.

The observation of a range of optical effects including the generation of structural colour has drawn the attention of many researchers and observers alike. For example, Hooke in 1665 noted that the remarkable pearly lustre of silverfish arises due to the manifold of reflecting surfaces of the transparent scales. Newton in his Opticks, published in 1704, described how the feathers of a bird exhibit a variety of

[8] It is noteworthy that recent historical research indicates that the law of refraction was known to Ibn Sahl prior to 984 and is accordingly credited with the discovery of the law of refraction.

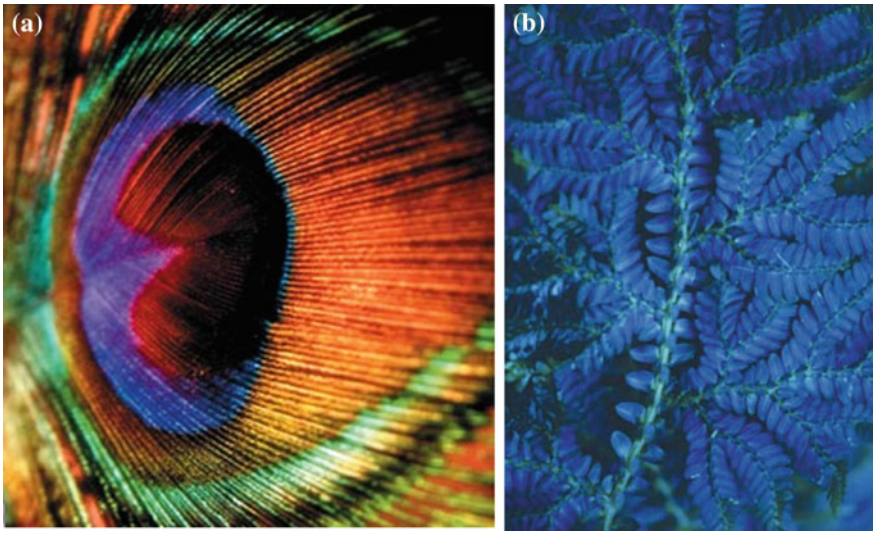

Fig. 2.3 Photonic crystals in nature. **a** The range of structural colours including browns in male peacock feathers [76]. *Image* Michael Shake/dreamtime.com. **b** Structural colour in flora illustrated by the *iridescent blue* in the fern-like tropical understory plants of the genus Selaginella [77]

colours when observed at different angles and attributed this to the transparency and slenderness of these very feathers. The physical basis of these natural examples of iridescence was clearly recognized as interference phenomena by Thomas Young who explained it about a century later in 1801—an important basis for the development of wave theory. Further, this is the basis of the phenomenon of diffraction—which is the resulting interference pattern of waves upon encountering obstacle(s)—first observed and characterized by Grimaldi in the seventeenth century followed by Fresnel's mathematical description in his 1815 publication. A few examples of photonic crystals occurring in nature are shown in Fig. 2.3.

The first observation of an antireflective film is attributed to Fraunhofer who discovered it by chance in 1817 as a result of tarnishing the surface of glass by nitric acid. Subsequently, upon observing the evaporation of a film of alcohol from a glass surface he noted that any transparent material being sufficiently thin will give rise to colour [78]. Similar observations were also made by Lord Rayleigh and further in his 1888 publication, *On the Remarkable Phenomenon of Crystalline Reflexion described by Prof. Stokes*, Lord Rayleigh proposes that bright colours of the chlorate of potash crystal are due to reflections at the twin planes of the crystal and that the fully formed colours are due to the presence of a number of alternating twin planes in the crystal [79]. These observations ultimately led Lord Rayleigh to conclude that the observed colours were a consequence of microscopic structure and hence coining the term structural colours. These basic studies have led to many studies examining multi-layered dielectric thin films including the Bragg mirror.

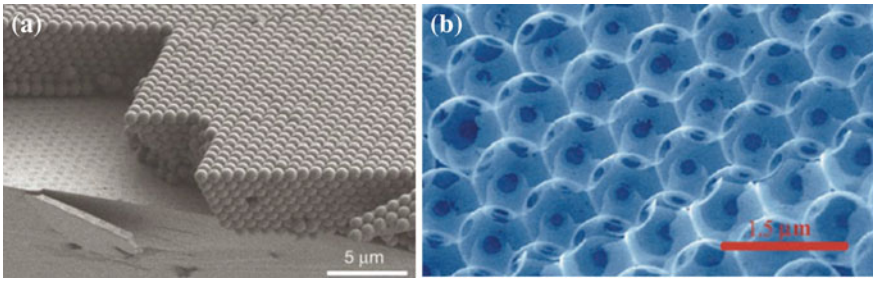

Fig. 2.4 Engineered photonic crystals. **a** Planar opal template using 855 nm spheres on a silicon wafer [80]. **b** Silicon inverse opal photonic crystal, [111] facet, with a complete three-dimensional bandgap near 1.5 μm [81]

A hundred years following the first observation of a 1 dimensional stop-band—a spectral range exhibiting large reflectivity—Yablonovitch and John published two independent papers that served to theoretically establish the possibility of an omni-directional stop-gap or a 3 dimensional photonic band gap [8, 9]. Similar to the periodic potential in semiconductor crystals that give rise to the electronic band structure, it was shown that periodic variation of the dielectric constant gives rise to a photonic band structure that exhibit allowed and disallowed modes of propagation for electromagnetic radiation—and hence the term photonic crystals which represents a class of periodic dielectrics or metallo-dielectrics wherein there are alternating regions of high and low dielectric media in one, two and/or three dimensions. Considering the diffractive basis of the physical effect, photonic crystals in the optical region are nanostructures with periodicity of the order of a fraction of the wavelength of light. Photonic crystals give rise to a whole host of fascinating phenomena which include suppression of spontaneous emission, light localization, photonic band gap, slow photons, the superprism effect, and low-loss waveguiding. A few examples of engineered photonic crystals are shown in Fig. 2.4.

The above outline highlights the foundational developments that have served to establish our understanding of optical and photonic phenomena which are critical for a multitude of optoelectronic applications. We now examine some of the early developments in silicon photovoltaics *vis-à-vis* optical coupling.

Paramount for the attainment of high efficiency operation in any photovoltaic device is complete optical absorption of the supra-bandgap portion of the solar spectrum. Complete optical absorption is challenged by thinning of the absorber material and exacerbated even further in indirect bandgap materials such as silicon. It is therefore clear that the employment of every possible technique that effectively serves to enhance the path length of the light and hence increase the probability of its absorption is essential.

St. John reported that through roughening of the silicon surface the number of internal reflections at the silicon-air interfaces can be increased and thus lead to light trapping and consequent intensity enhancement [82]. While such early studies were motivated by microelectronic applications, Redfield reported that maximizing the number of passes directly impacts the conversion efficiency of silicon solar cells and

accordingly multiple reflections are essential [83]. Yablonovitch and Cody using a statistical mechanical analysis showed that maximum possible enhancement in path length (relative to the thickness of the absorber) is $4n^2$ where n is the index of refraction of the weakly absorbing material such as silicon—having taken into account all oblique angle paths (factor of 2) and reflections from the rear interface (another factor of 2). These studies suggest that so long as the surface is sufficiently strongly textured, random or precisely grooved, an enhancement limit of $4n^2$ can be approached, which is approximately 50 for silicon [84]. Sheng, Bloch and Stepelman subsequently report that the use of 1-D or 2-D periodic patterning can render wavelength-selective absorption in thin film silicon [85]. Sheng et al. exemplify that analogous to the periodic potential in a crystal that gives rise to 'peaks' in the particle/electron density of states at a certain set of frequencies (otherwise referred to as van Hove singularities) and 'gaps' at others, the use of periodic gratings gives rise to a similar set of photon density of states. Through an appropriate selection of grating parameters the resonant photon density of states can be positioned within the optical gap of the material, effectively increasing the number of photon states above the absorption edge albeit at the expense of the states in the neighbouring non-absorbing region. Thus, in the absorbing region the density of states exceeds the n^2 limit and hence yielding further enhancement in light trapping.

The above described represent some of the first key studies that illustrated the enormous potential of modulating the flow of light in silicon solar cells through physical structuring of the absorbing material. A host of studies followed that investigated the use of patterned surfaces, gratings, inverted pyramids, tilted inverted pyramids, metallic back reflectors, introduction of dielectric interlayers between the metallic back reflector and the silicon absorber in an effort to maximize the absorption of the impinging solar radiation. These developments—together with advances in the electronic design of the devices as well as enhancements in device fabrication which have included the development of optimal passivation and effective carrier extraction techniques—have led to record photovoltaic conversion efficiencies in crystalline silicon albeit in relatively thick absorbers. Over the last couple of decades there has been much research to further develop novel photonic constructs at the wavelength and sub-wavelength scale so as to effectively tune spectral localization and thus attain complete optical absorption in both thin crystalline silicon and thin film silicon solar cells. We now examine some of these recent advances in the field.

2.3 Nano Architectures in Silicon Photovoltaics: Recent Advances

2.3.1 Introduction

Today, state-of-the-art commercial crystalline silicon solar cells with record photovoltaic efficiencies in the 22–24 % range have silicon wafer thicknesses in the range

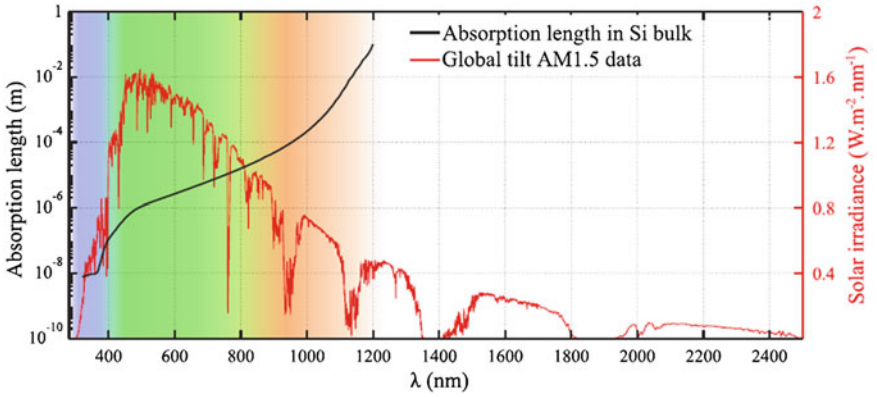

Fig. 2.5 The absorption length of crystalline silicon juxtaposed against the AM1.5G solar irradiance. The *blue*, *green*, and *red* coloured regions indicate the region with the highest optical absorption, the region with the highest solar irradiance, and the region with absorptions lengths in excess of 100 μm, respectively [86]

of 100–150 μm. While this is a remarkable achievement in relation to the foundational developments by Russel Ohl in 1941, recognition of the potential of developing silicon[9] solar cells with comparable efficiencies but some two orders of magnitude thinner has driven research towards the pursuit of a myriad of nano-photonic and plasmonic paradigms. An essential characteristic of this quest is efficacious light trapping and optical absorption so as to attain the ultimate photogenerated charge density and hence conversion efficiency; this is well illustrated in Fig. 2.5 which contrasts the absorption length in crystalline silicon against the AM1.5 solar spectrum.

Much of the research over the last decade has been optical in nature and hence independent of the electrical requirements of the device. Nonetheless, integrated designs have also been investigated and inevitably reveal the magnitude of the challenge. In the following sections we provide a selected overview of some of the recent advances in the field of crystalline silicon and amorphous silicon photonic crystal photovoltaics.

2.3.1.1 Photonic Crystals

The term 'photonic crystal' was coined to reflect the analogous behaviour of electromagnetic waves in three-dimensional periodic dielectric structures [8, 9] with that of electron waves in three-dimensional periodic potentials [87, 88]. Some of the earliest studies in photonic crystals were motivated by the objective of developing photonic bandgap materials that would permit control over radiative emission and light localization and thus usher an era of the three-dimensional all-optical micro-chip —the

[9] As well as other photovoltaic materials.

light computer [10, 89, 90]. These studies, in addition to the existing foundation of spectrally selective interference filters or Bragg stacks, spurred research into nano-structured silicon photonic crystal photovoltaics [91–94]. Within this framework, photonic crystals can be employed in photovoltaic cells in a variety of ways which can be principally divided into two categories. First, where the photonic crystal is outside the photoactive region and serves the function of omni-directional reflection and diffraction of quasi guided-modes into the unpatterned silicon absorber; examples of this application include back-reflector and intermediate reflectors. And second, the photoactive region is patterned into a photonic crystal itself so as to couple light into the quasi-guided modes within the absorber. Both approaches serve to enhance light intensity and hence photoabsorption [95].

2.3.1.2 Photonic Crystals in Crystalline Silicon PV

One of the early theoretical studies reporting on the use of photonic crystals in thin crystalline silicon (c-Si) solar cells by Bermel et al. [38] show that the use of nano-structured elements effect wave-optic light-trapping mechanisms which in contrast to geometric optics can be effectively tuned to enhance absorption in the near infrared part of the spectrum where the absorption coefficient in silicon is low owing to its indirect-gap band structure. Three cell concepts based on 2 μm thick c-Si are considered, as shown in Fig. 2.6. All cell structures consist of the silicon absorber and an anti-reflective coating on the front light-facing side, while the rear surfaces of the cells are structured with different back reflectors. In Fig. 2.6a the back reflector consists of a distributed Bragg reflector (DBR) comprising of ten thick bi-layers of c-Si and SiO_2 having indices of 3.5 and 1.5, respectively, with a period of 150 nm. The DBR parameters are chosen so as to reflect strongly in the near-IR. The overall cell efficiency is reported to be 12.44 % which is comparable to that with a plain aluminum back reflector of 12.72 %. In contrast, in the second design shown in Fig. 2.6b a 1D grating is introduced in the low-index SiO_2 layer immediately adjacent to the c-Si absorber. In addition to reflection, the grating serves to introduce diffractive modes into the absorber and hence extend the path length of the light. Optimization of the structure leads to an eight bilayer DBR having a period of 165 nm and a 1D grating with a period of 264 nm and etch depth of 67 nm for a 2 μm thick c-Si absorber, and hence a conversion efficiency of 15.42 %. The enhancement in absorption in c-Si absorbers ranging from 2 to 32 μm in thickness are shown in Fig. 2.6d. As expected, the enhancement is most significant for the thinnest absorber layer, attaining an almost 5-fold increase in the near-IR absorption. The third design, shown in Fig. 2.6c, replaces the back reflector with an inverse opal photonic crystal comprising the absorber material itself.[10] In this case not only are reflection

[10] An opaline structure consists of silica spheres appropriately close-packed to form a crystalline lattice, while an inverse opal architecture comprises the interstices of the opaline structure appropriately filled with a suitable dielectric material (wherein the spherical volume associated with the opal form the void with relative permittivity of 1).

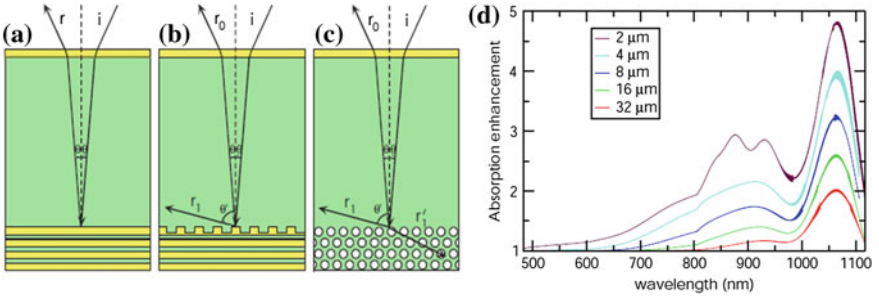

Fig. 2.6 Solar cell structures consisting of crystalline silicon absorber, an antireflective coating on the light facing side, and three different back reflectors. **a** Back reflector consisting of a distributed Bragg reflector. **b** Back reflector comprising a DBR and a 1D grating. **c** Back reflector comprising an inverse opal photonic crystal containing a triangular lattice of air holes. **d** Enhancement in the spectral absorption as a result of introducing a 1D grating into a DBR for c-Si absorber thicknesses ranging from 2 to 32 μm [38]

and diffractive modes contributing to photogeneration, but additional modes that penetrate into the photonic crystal absorber also contribute to the overall absorption. In this instance, the optimized efficiency is 15.73 % with 8 periods. It is worth noting that introduction of an optimized 2D grating however leads to an efficiency of 16.32 % with a 4 bilayer DBR; this structure is referred to as a textured photonic crystal back reflector where the DBR is a 1D photonic crystal. Zeng et al. fabricated a 5 mm thick c-Si photovoltaic device and showed a short circuit current density enhancement of 19 % compared to a 28 % scattering matrix method prediction [96].

In a similar vein, O'Brien et al. [40] demonstrated the use of an opaline photonic crystal (PC) as a back-reflector to enhance the photoabsorption in thin film amorphous silicon (Fig. 2.7a). Through variation of the diameter of silica spheres, ranging from 190 to 343 nm, the [111] stop-gap is tuned from its centered value of $\lambda = 410$ nm to $\lambda = 740$ nm; the opaline photonic crystal has a narrow stopgap of $\Delta\omega/\omega$ of 5.5 % in this direction between the second and third photonic bands. For a 250 nm thick amorphous silicon film an enhancement of 2.5 is observed compared to a scalar wave approximation (SWA) value of 3 (Fig. 2.7b). Further, it is shown that strong resonant modes exist within and outside of the stopgap which occur due to scattering at the photonic crystal surface and that these planar resonant modes propagate along the plane of the film and thus enhance absorption. In a subsequent study, O'Brien et al. [42] report on a similar opaline photonic crystal back reflector adjoining a 10 μm thick crystalline silicon wafer and show a 1.5 fold enhancement in absorption. In this study they also show that the introduction of an intervening electronic element, such as a transparent conducting oxide, in aid of creating a complete photovoltaic device very quickly diminishes the optical benefits of a contiguous photonic crystal back reflector (Fig. 2.7c), thus calling for the need of structuring the conducting back-contact itself in the form of a photonic crystal.

Chutinan et al. [97] investigated the prospect of configuring thin crystalline silicon solar cells such that the absorbing layer is a photonic crystal. The study considers

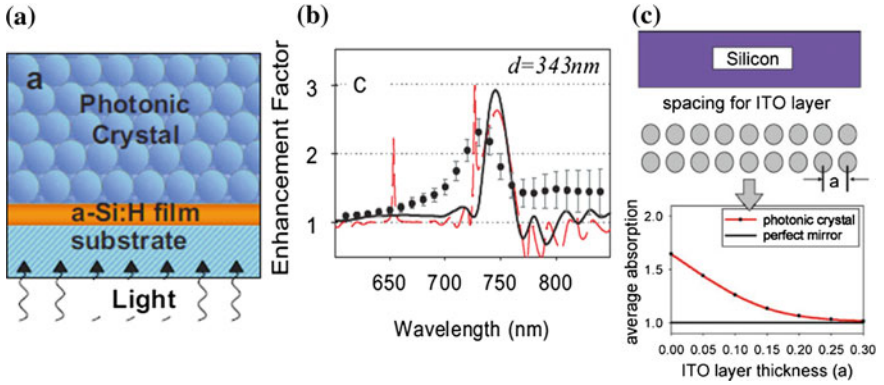

Fig. 2.7 Photonic crystal back reflectors on thin silicon absorbers. **a** Opaline photonic crystal on 250 nm thin a-Si:H film [40]. **b** Enhancement in the photoconductivity of the PC-a-Si:H construct (*d* is the opal diameter, *black curve* is the scalar wave approximation (SWA), and *red curve* is the finite-difference time-domain (FDTD) calculation) [40]. **c** An illustration of the loss in absorption enhancement due to the presence of an intervening indium tin oxide (ITO) layer between the c-Si absorber and PC back reflector [42]

crystalline silicon layers as thin as 2 μm such that the volume of silicon is maintained constant for each cell design for a given thickness. As a reference, optimal standard cell designs are evaluated where the cell comprises an antireflective coating on the light facing (front) side and a grating on the back side along with a perfect back reflector. The 2D photonic crystal cell architecture consists of a square lattice of square silicon rods in an air background (Fig. 2.8a); further, the light facing side has an appropriate light coupler (to couple the incoming light into the photonic crystal). In addition, as in the reference cell, the frontside has an antireflective coating and the backside has a grating and a perfect back reflector. The cell efficiencies of the photonic crystal designs are shown to exceed the standard designs with the greatest increase realized for the 2 μm case—the PC design showing an overall efficiency increase of 11 % over the standard design.

Mallick et al. [98] also investigated 2D silicon photonic crystal architectures albeit with an even thinner crystalline silicon thickness of 400 nm. The design consists of a double layer silicon photonic crystal architecture (Fig. 2.8b). The active double layer has an antireflection coating on the front side and a 400 nm thick SiO_2 layer on the back side, along with a metal layer that ensures double-pass reflection. A square lattice of cylindrical holes are introduced in the double layer 2D PC; the top layer has a set of holes which are smaller in diameter relative to those in the bottom layer, thus providing a greater degree of freedom in attaining an optimal design. The antireflective coating on the top along with the upper layer PC is also perforated. The optimal structure exhibits an average enhancement in absorption of approximately 2.5 compared to a standard flat cell with equivalent volume of c-Si when averaged over all angles; the maximum achievable photocurrent density increases 3.1 fold from 7.1 to 21.8 mA/cm^2 in comparison to the Yablonovitch limit of 26.5 mA/cm^2.

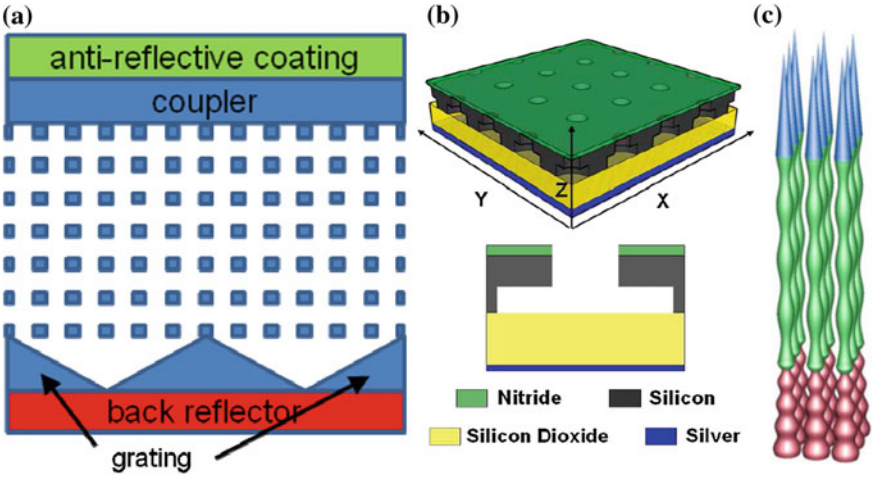

Fig. 2.8 Silicon photonic crystal absorbers. **a** 2D PC square lattice of square rods [97]. **b** 2D double layer photonic crystal lattice of holes [98]. **c** Radius-modulated nanowire integrating nanocones for antireflection, cubic photonic crystal for parallel interface refraction, and photonic back reflector [86]

Demesy et al. [86] have recently reported a silicon nanowire photonic crystal architecture that through nanostructuring integrates the optical effects of antireflection, light trapping and back reflection (Fig. 2.8c). Using a 1 μm thick crystalline silicon layer, the active region is shaped into a 3D simple-cubic photonic crystal consisting of radius-modulated silicon nanowires embedded within SiO_2 and placed on a quartz substrate. The top of the nanowires facing the incoming light are conical in shape with a linear change in radius wherein the nanocones provide effective broadband coupling of the incident light as well as good absorption at short wavelengths. The mid-section of the nanowire is a simple cubic photonic crystal that exhibits effective light trapping owing to parallel interface refraction resonances [99], deflecting light laterally into slow group velocity modes, thus leading to up to 150 fold enhancement in light intensity. The bottom section of the nanowire is shaped to create a 1D photonic back reflector. The modulated silicon nanowire photonic crystal structure is shown to trap and absorb approximately 75 % of the incident solar radiation in the 400–1,200 nm range. In a subsequent study, Deinega et al. [100] investigate this architecture for optimal junction and contact geometries, having solved Maxwell's equations and the continuity-transport equations, and show a 20 % enhancement in conversion efficiency compared to an equivalent volume of plain silicon.

In concluding this section it is important to note that while the above investigations highlight the salient aspects of integrating photonic crystals in silicon photovoltaics, there is an enormous body of recent allied research that is worthy of mention. We direct the interested readers to a selected set of publications in the open literature including some of the earliest research into coherent scattering of light in photovoltaics [101–105]. Moreover, we also point the readers to a body of research on

patterning of silicon surfaces including recent forays into nano-structuring where wave-optic light coupling techniques are being explored to effect light trapping in silicon PV [106–111].

2.3.1.3 Photonic Crystals in Thin Film Silicon PV

In contrast to crystalline silicon photovoltaics, which is a predominantly wafer based platform, thin film silicon photovoltaics is an essentially bottom-up low-temperature synthesis approach encompassing single and multiple junction hydrogenated amorphous silicon solar cells as well as the so-called dual-junction micromorph cell. Amicromorph cell consists of a hydrogenated amorphous silicon (a-Si:H) top-cell with a bandgap of ∼1.7 eV and a micro/nano-crystalline silicon (μc-Si:H) bottom-cell with a bandgap of ∼1.1 eV. The all-silicon micromorph thin film cell[11] has the potential of attaining the near-term target of a stabilized photovoltaic conversion efficiency exceeding 15 %, however, effective light harvesting and device engineering are required; it is noteworthy that theoretical efficiencies are predicted to be at least a factor of two higher [112].

The thin film micromorph device consists of the a-Si:H and μc-Si:H cells connected in series such that the output voltage of the micromorph is the sum of its two individual component cells. An essential requirement for optimal energy conversion in such multi-junction cells is matched cell current densities. The micromorph cells are top-limited, that is, their output is limited by the relatively lower current density generated in the top a-Si:H cell as compared to the higher current density generated by the bottom μc-Si:H based cell. While the top cell current density can be amplified by increasing its cell thickness, a thicker a-Si:H cell inevitably suffers from light induced degradation as a result of the Staebler-Wronski effect (SWE) and associated drop in the internal electric field intensity. Light trapping schemes have been implemented to increase photon absorption in the upper a-Si:H cell.

One commonly used strategy is to deposit a transparent conducting oxide (TCO) layer between the a-Si:H and μc-Si:H junctions. In this configuration the TCO layer acts as an intermediate reflector (IR), ideally causing Fabry-Perot oscillations that return incident photons of energy greater than ∼1.7 eV to the a-Si:H cell in order to enhance the current generated in the upper cell while transmitting photons of lesser energy to the underlying μc-Si:H cell.

A variety of materials and structures as possible alternatives for the fabrication of effective intermediate reflectors (IRs) have recently been investigated. Asymmetrically textured ZnO IRs, wherein the top surface has feature sizes of ∼300 nm to efficiently scatter blue-green light while the bottom surface has larger features to

[11] 'All-silicon' emphasizes the intrinsic hydrogenated amorphous silicon and intrinsic microcrystalline silicon absorber layers in the top and bottom cells, respectively, and the fact that there is typically no germanium alloying for bandgap engineering. The occlusion of germanium in amorphous silicon has been used to successfully fabricate triple-junction thin film amorphous Si cells; however this approach is fraught with a whole host of challenges and the micromorph is deemed to be a more promising alternative.

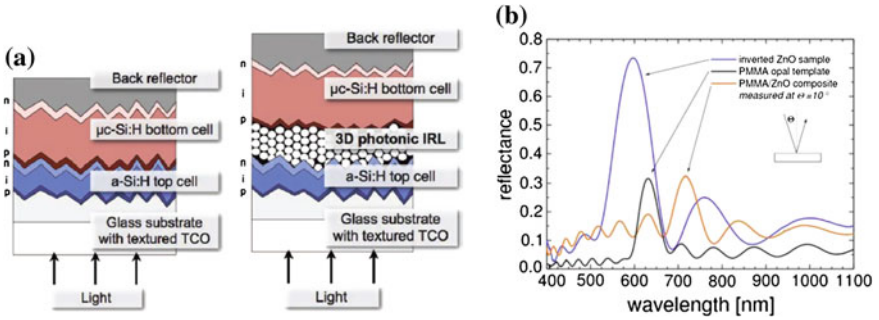

Fig. 2.9 Three dimensional photonic crystal intermediate reflector in the micromorph cell. **a** Schematic diagrams of the standard micromorph cell without an intermediate reflector and with an inverted opal photonic crystal intermediate reflector [44]. **b** Spectral reflectance profile of the inverted ZnO opal contrasted against the reflectance spectra of PMMA opaline PC and the PMMA composite wherein the interspaces are infiltrated with ZnO [41]

scatter red light, have been used to fabricate 11.2 % (initial) efficient micromorph cells on flexible plastic substrates [113]. Another approach has been to fabricate micromorph cells with doped silicon oxide IRs (SOIRs), motivated by the advantage of being able to deposit SOIRs in one and the same reactor as the micromorph cell itself; first cell with conversion efficiency of 12.2 % (initial) has been reported [114].

More recently, Bielawny et al. have proposed the utilization of three-dimensional photonic crystal IRs in the form of inverted aluminum doped zinc oxide (ZnO:Al) opals [41, 44, 93]. The 3D PC IR in a micromorph cell is illustrated in Fig. 2.9a. The top a-Si:H cell is grown conformally over the textured TCO on glass substrate followed by the synthesis of the inverted ZnO:Al opaline PC. The bottom μc-Si:H cell and a back contact which doubles as an optical reflector are deposited subsequently to complete the device fabrication. Typical measured spectral reflectance for the inverted ZnO:Al opal is shown in Fig. 2.9b, indicating the potential of high broadband enhancement in light trapping. The measured reflectance spectra for polymethyl-metacrylate (PMMA) and PMMA-ZnO:Al composite are also shown and suggest the PC synthesis process steps. Detailed analysis have shown that the PC provides photonic stop gap reflectance as well as diffractive modes, resulting in the overall enhancement of the photocurrent density in the top cell. Experimentally, an enhancement in the short circuit current density of the amorphous silicon top cell of 24.5 % has been reported which compares well with the theoretical prediction of 28 %.

In contrast, O'Brien et al. have carried out a comparative investigation of photonic crystal intermediate reflectors utilizing μc-Si/ZnO Bragg-reflector constructs and ZnO inverted opals in micromorph cells [115]. The cell configurations with the μc-Si/ZnO Bragg-reflector and ZnO inverted opal intermediate reflectors are shown in Fig. 2.10a, b, respectively. The top a-Si:H cell is 100 nm thick while the bottom microcrystalline cell is infinitely thick; use of a 2 μm thick μc-Si:H cell shows only a 1 % relative increase in the top cell current. The absorption/reflectance profiles for

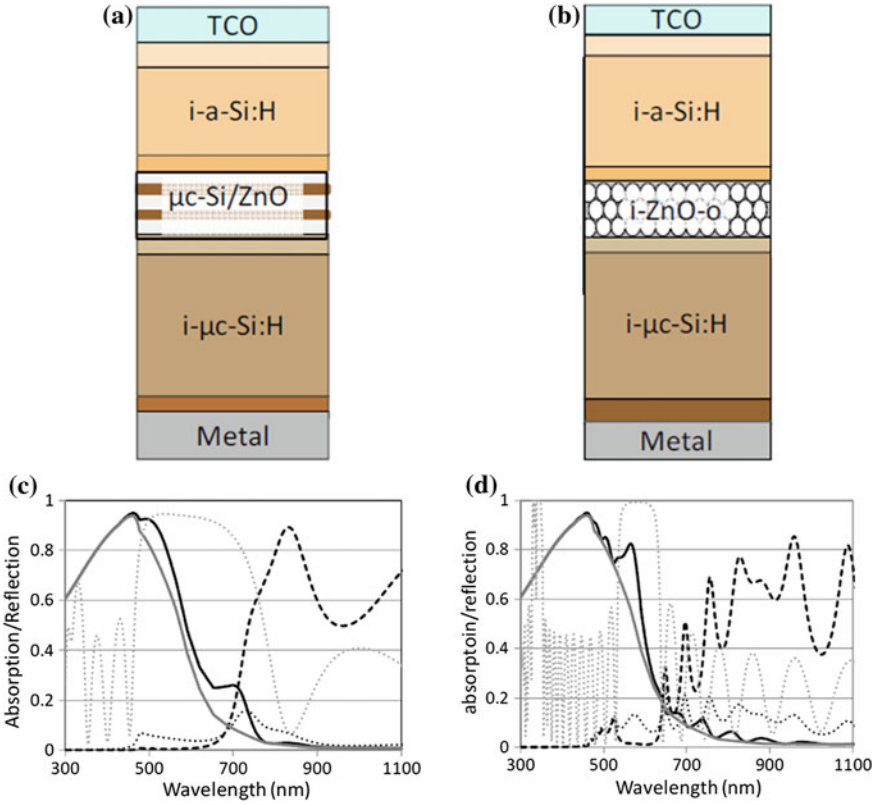

Fig. 2.10 Micromorph cells utilizing photonic crystals as intermediate reflectors. **a** Schematic diagrams of micromorph cells using a ZnO/μc-Si:H Bragg-reflector IR (**a**) and a ZnO inverted opal IR (**b**). Absorption and reflection profiles for the two cell configurations are shown in (**c**) and (**d**), respectively. The absorption spectrum for the top 100 nm thick a-Si:H cell in a reference micromorph tandem cell without an IR is shown as a *solid grey line* in (**c**) and (**d**). The absorption spectra for the top 100 nm thick a-Si:H in cells (**a**) and (**b**) are shown as *solid black lines* in (**c**) and (**d**), respectively. The absorption in the PCs and the underlying μc-Si:H cells are shown as the *dotted* and *dashed black lines*, respectively. The reflectance from a three and half bilayer ZnO/μc-Si:H Bragg-reflector and reflectance from a 13-layered ZnO inverted opal reflector, similar to configurations where the medium above and below the reflector is air and μc-Si:H, respectively, are plotted as *dotted grey lines*, respectively; absorption of the IRs in these reflectance spectra have been neglected in order to emphasize their reflectance peaks [115]

the μc-Si/ZnO Bragg-reflector and ZnO inverted opal IR based micromorph cells are shown in Fig. 2.10c, d, respectively. Both cell configurations indicate enhanced absorption in the top cell relative to that in a reference micromorph cell without an IR. The μc-Si/ZnO Bragg-reflector IR based micromorph cell indicates a 20 % increase in the top cell current while the ZnO inverted opal IR based micromorph cell shows a 13 % increase in its top cell current. The larger increase with the Bragg IR based cell is due to its larger stop-gap (evident by reflectance of the PC IRs represented by the

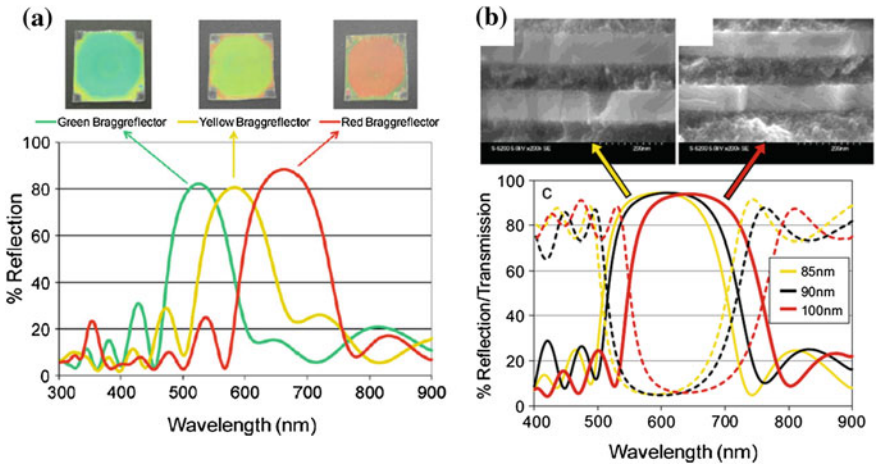

Fig. 2.11 Reflectance/transmittance spectra of 1D selectively transparent and conducting photonic crystals synthesized from bilayers of nanoparticle and transparent conducting oxide films. **a** Reflectance spectra, and corresponding photographs, of *red*, *yellow* and *green* STCPCs with Bragg peak's at approximately 670, 580 and 520 nm, respectively; these STCPCs were fabricated using antinomy tin oxide nanoparticles and indium tin oxide films. **b** Reflectance (*solid*) and transmittance (*dashed*) spectra of 5 bilayer STCPCs having equivalent ITO film thicknesses of 85, 90 and 100 nm; SEM cross-sectional viewgraphs of STCPS with 85 and 100 nm thicknesses are shown above the plot [43, 45]

grey dotted lines in Fig. 2.10c, d with $\Delta\omega/\omega$ of ~45 % for the Bragg and ~14 % for the opal IRs, respectively), the Bragg IR being optically thinner, and the opaline IR exhibiting greater absorption losses. Specifically, the Bragg IR micromorph shows a photogenerated current density of 13.8 mA/cm^2 in the top cell and 14.9 mA/cm^2 in the bottom cell.

More recently O'Brien et al. have reported the development of conducting photonic crystals, also known as selectively transparent and conducting photonic crystal (STCPC), amenable to a variety of optoelectronic devices including silicon micromorph solar cells [43]. The 1D STCPCs consist of bilayers of sub-wavelength nanoparticles and transparent conducting films each of the order of 100 nm in thickness which together provide the index contrast and an electrically continuous structure. In their first report, the STCPCs specifically consisted of 25 nm antimony tin oxide (ATO) nanoparticle films and sputtered indium tin oxide (ITO) films. The reflectance spectra of these STCPCs are shown in Fig. 2.11a, illustrating the wide band tunability of these conducting photonic crystals that have sheet resistances of less than 88 Ω/□ and 55 Ω/□ for 3.5 and 5.5 bilayers, respectively. In a subsequent development, the properties of the STCPCs are improved further through the utilization of 10 nm silica nanoparticles which serve to increase the index contrast as well as overcome the parasitic absorption losses in the ATO nanoparticles [45]. The reflectance spectra of these silica nanoparticle STCPCs, shown in Fig. 2.11b, indicate peak transmissivities of 95 % with significantly wider reflection bands that are easily

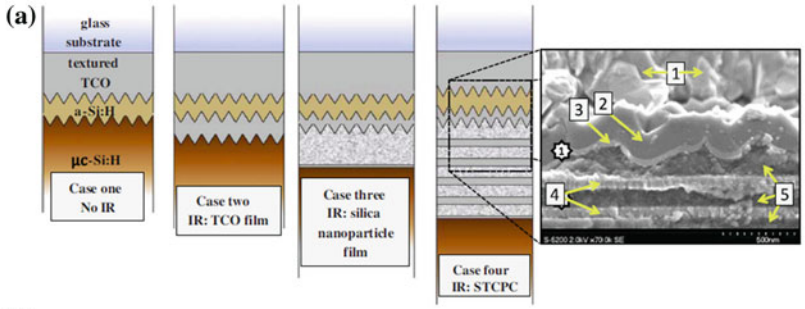

(b)

Type of intermediate reflector	$\theta_s = 0°$		$\theta_s = 45°$	
	$I_{a\text{-Si:H}}$ (mA/cm^2)	$I_{\mu c\text{-Si:H}}$ (mA/cm^2)	$I_{a\text{-Si:H}}$ (mA/cm^2)	$I_{\mu c\text{-Si:H}}$ (mA/cm^2)
Case 1: No IR	10.57	27.40	10.33	26.65
Case 2: ITO film	11.17	25.51	11.01	24.32
Case 3: Silica nanoparticle film	11.60	20.38	11.56	19.04
Case 4: STCPC IR (λ_p = 560 nm)				
1 bilayer	12.19	20.49	12.10	20.32
3 bilayers	12.72	18.48	12.33	19.06
5 bilayers	12.83	18.91	12.33	18.76
Case 4: STCPC IR (λ_p = 620 nm)				
1 bilayer	12.13	19.00	12.20	18.79
3 bilayers	12.57	17.04	12.69	16.77
5 bilayers	12.65	16.34	12.78	17.11

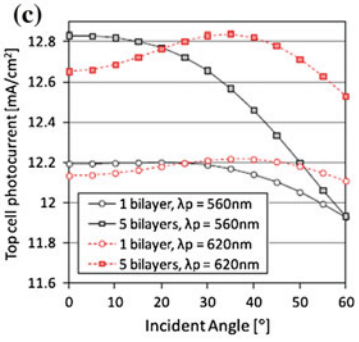

Fig. 2.12 **a** Schematic diagram of the micromorph cells with different intermediate reflectors examined using the scattering matrix method. The reference case has no IR while cases 2–4 consist of an ITO film IR, silica nanoparticle film IR, and STCPC IR, respectively. The SEM cross-sectional view corresponding to case 4 illustrates the planarizing effect of the silica nanoparticles; in this figure, *1* is the textured TCO, *2* is the 150 nm thick a-Si:H film, *3* is the conformal 50 nm thick ITO film, *4* points to the ITO films within the STCPC and *5* points to the silica nanoparticle films also within the STCPC. **b** Summary of the short-circuit current densities in the top a-Si:H cell and the bottom μc-Si:H cell for AM1.5 illumination at normal incidence and at 45° from the normal corresponding to the different cases illustrated in (**a**). **c** The top cell short circuit current densities as a function of the angle of incidence for micromorph cells with different STCPC IRs [45]

tuned. Further, contrary to conventional wisdom, the electrical conductivity of these films is even greater with sheet resistance of 15 Ω/□ for 5.5 bilayer structures; the development of a continuous electrical pathway is attributed to infiltration and percolation of ITO in the interstices of the essentially close-packed silica nanoparticle films and any shunts due to imperfections/holes in the nanoparticle films.

Integration of these STCPCs as intermediate reflectors in micromorph cells have been investigated using the scattering matrix method and compared against the reference cases of no intermediate reflector, an ITO thin film IR and a silica nanoparticle film IR. A schematic of the four cases is shown in Fig. 2.12a and a corresponding summary of the photogenerated current densities is shown in Fig. 2.12b. Incorporation of STCPC IRs leads to photocurrent density enhancements in top cell, relative to the case of no IR, of 15.3, 20.3 and 21.4 % for 1, 3 and 5 bilayer STCPCs, respectively,

where the Bragg peak is at 560 nm and the 1 sun illumination is at normal incidence. Photocurrent enhancements are also evident for off-normal incidence of 45° and in particular the enhancement is equally large for STCPCs tuned with a Bragg peak at 620 nm. The photocurrent densities in the top cell as a function of the incidence angle, for STCPCs with the two Bragg peaks, are shown in Fig. 2.12c; the curves indicate the ability to tune STCPCs to attain directionally-invariant enhancement. It is also interesting to observe the planarizing effect of the STCPC (see Fig. 2.12a, case 4); specifically, the silica nanoparticles fill the texture in the underlying TCO on the glass substrate and thus present a much smoother surface for the growth of microcrystalline silicon with potentially ameliorative implications.

The above presentation highlights some of the recent efforts to integrate photonic crystals in thin film silicon photovoltaics. As in the crystalline silicon case, significant research into various surface patterning constructs to effect light trapping have been carried out and we direct the interested reader to a selected set of articles in this body of literature [116–119]. We also point the interested reader toward allied integration of photonic crystals and nanostructures in other photovoltaic material systems [120–123].

2.4 Future Outlook

The remarkable surge of fundamental research activity in the field of nanostructured materials over the last decade coupled with the effort to apply these emerging basic insights to photovoltaics bodes favourably for the ultimate attainment of versatile and economic generation of solar electricity. Ground breaking research activities in plasmonic metamaterials, use of topology optimization techniques based on genetic algorithms, and the drive towards monolithic integration is expected to create an exciting future for a range of photovoltaic materials including silicon [124–126]. It is anticipated that silicon will continue to evolve in its applicability with new advances in science and technology considering its obvious advantages, mature manufacturing platform and its abundance.

Acknowledgments The author gratefully acknowledges copyright holders' granting permission to reproduce selective figures and tables (which have been clearly cited) in this chapter.

References

1. J.C. Maxwell, Proc. R. Soc. Lond. A **13**, 531 (1864)
2. J.C. Maxwell, Philos. Trans. R. Soc. B **155**, 459 (1865)
3. R.P. Feynman, *Quantum Electrodynamics* (W. A. Benjamin, New York, 1961)
4. C. Cohen-Tannoudji, J. Dupont-Roc, G. Grynberg, *Photons and Atoms: Introduction to Quantum Electrodynamics* (Wiley, New York, 1989)
5. V.G. Veselago, Sov. Phys. Uspekhi-Ussr **10**, 509 (1968)

6. D.R. Smith, J.B. Pendry, M.C.K. Wiltshire, Science **305**, 788 (2004)
7. M. Memarian, G.V. Eleftheriades, Light Sci. Appl. **2**, e114 (2013)
8. S. John, Phys. Rev. Lett. **58**, 2486 (1987)
9. E. Yablonovitch, Phys. Rev. Lett. **58**, 2059 (1987)
10. J.D. Joannopoulos, S.G. Johnson, J.N. Winn, R.D. Meade, *Photonic Crystals: Molding the Flow of Light*, 1st edn. (Princeton University Press, Princeton, 1995) (2nd edn, 2008)
11. D.W. Prather, S. Shi, A. Sharkawy, J. Murakowski, G.J. Schneider, *Photonic Crystals: Theory, Applications, and Fabrication* (Wiley, Hoboken, 2009)
12. V.M.N. Passaro, *Advances in Photonic Crystals* (InTech, Rijeka, 2013)
13. W.L. Barnes, A. Dereux, T.W. Ebbesen, Nature **424**, 824 (2003)
14. H.A. Atwater, Sci. Am. **296**, 56 (2007)
15. S.A.A. Maier, *Plasmonics: Fundamentals and Applications* (Springer, New York, 2007)
16. G. Cao, *Nanostructures and Nanomaterials: Synthesis, Properties and Applications* (Imperial College Press, London, 2004)
17. G.A. Ozin, A.C. Arsenault, L. Cademartiri, *Nanochemistry: A Chemical Approach to Nanomaterials* (Royal Society of Chemistry, Cambridge, 2009)
18. E. Becquerel, Comptes rendus de l'Académie des Sciences **9**, 561 (1839)
19. D.M. Chapin, C.S. Fuller, G.L. Pearson, J. Appl. Phys. **25**, 676 (1954)
20. M.A. Green, Prog. Photovoltaics **17**, 183 (2009)
21. M. Taguchi, A. Yano, S. Tohoda, K. Matsuyama, Y. Nakamura, T. Nishiwaki, K. Fujita, E. Maruyama, IEEE J. Photovoltaics **4**, 96 (2013)
22. A. Luque, S.E. Hedgedus, *Handbook of Photovoltaic Science and Technology* (Wiley, Chichester, 2011)
23. A. McEvoy, T. Markvart, L. Castañer, *Solar Cells: Materials, Manufacture and Operation* (Elsevier, Amsterdam, 2013)
24. M.A. Green, K. Emery, Y. Hishikawa, W. Warta, E.D. Dunlop, Prog. Photovoltaics **21**, 1 (2013)
25. K.E. Kalyanasundaram, *Dye-Sensitized Solar Cells* (EPFL Press, Lausanne, 2010)
26. A. Yella, H.W. Lee, H.N. Tsao, C.Y. Yi, A.K. Chandiran, M.K. Nazeeruddin, E.W.G. Diau, C.Y. Yeh, S.M. Zakeeruddin, M. Gratzel, Science **334**, 629 (2011)
27. L.Y. Han, A. Islam, H. Chen, C. Malapaka, B. Chiranjeevi, S.F. Zhang, X.D. Yang, M. Yanagida, Energy Environ. Sci. **5**, 6057 (2012)
28. N. Tétreault, M. Grätzel, Energy Environ. Sci. **5**, 8506 (2012)
29. C. Brabec, V. Dyakonov, U. Scherf, (eds.), *Organic Photovoltaics: Materials, Device Physics, and Manufacturing Technologies* (WILEY-VCH, Weinheim, 2008)
30. M. Wright, A. Uddin, Sol. Energy Mater. Sol. Cells **107**, 87 (2012)
31. A.G. Pattantyus-Abraham, I.J. Kramer, A.R. Barkhouse, X.H. Wang, G. Konstantatos, R. Debnath, L. Levina, I. Raabe, M.K. Nazeeruddin, M. Gratzel, E.H. Sargent, Acs Nano **4**, 3374 (2010)
32. O.E. Semonin, J.M. Luther, S. Choi, H.Y. Chen, J.B. Gao, A.J. Nozik, M.C. Beard, Science **334**, 1530 (2011)
33. J. Burschka, N. Pellet, S.J. Moon, R. Humphry-Baker, P. Gao, M.K. Nazeeruddin, M. Gratzel, Nature **499**, 316 (2013)
34. M.Z. Liu, M.B. Johnston, H.J. Snaith, Nature **501**, 395 (2013)
35. A.E. Al-Ahmadi, *Quantum Dots—A Variety of New Applications* (InTech, Rijeka, 2012)
36. L. Mangolini, E. Thimsen, U. Kortshagen, Nano Lett. **5**, 655 (2005)
37. M.L. Mastronardi, E.J. Henderson, D.P. Puzzo, Y.L. Chang, Z.B. Wang, M.G. Helander, J.H. Jeong, N.P. Kherani, Z.H. Lu, G.A. Ozin, Small **8**, 3647 (2012)
38. P. Bermel, C. Luo, L. Zeng, L.C. Kimerling, J.D. Joannopoulos, Opt. Express **15**, 16986 (2007)
39. A. Polman, H.A. Atwater, Nat. Mater. **11**, 174 (2012)
40. P.G. O'Brien, N.P. Kherani, S. Zukotynski, G.A. Ozin, E. Vekris, N. Tetreault, A. Chutinan, S. John, A. Mihi, H. Miguez, Adv. Mater. **19**, 4177 (2007)

41. A. Bielawny, J. Upping, P.T. Miclea, R.B. Wehrspohn, C. Rockstuhl, F. Lederer, M. Peters, L. Steidl, R. Zentel, S.M. Lee, M. Knez, A. Lambertz, R. Carius, Phys. Status Solidi A-Appl. Mater. Sci. **205**, 2796 (2008)
42. P.G. O'Brien, N.P. Kherani, A. Chutinan, G.A. Ozin, S. John, S. Zukotynski, Adv. Mater. **20**, 1577 (2008)
43. P.G. O'Brien, D.P. Puzzo, A. Chutinan, L.D. Bonifacio, G.A. Ozin, N.P. Kherani, Adv. Mater. **22**, 611 (2010)
44. J. Upping, A. Bielawny, R.B. Wehrspohn, T. Beckers, R. Carius, U. Rau, S. Fahr, C. Rockstuhl, F. Lederer, M. Kroll, T. Pertsch, L. Steidl, R. Zentel, Adv. Mater. **23**, 3896 (2011)
45. P.G. O'Brien, Y. Yang, A. Chutinan, P. Mahtani, K. Leong, D.P. Puzzo, L.D. Bonifacio, C.W. Lin, G.A. Ozin, N.P. Kherani, Sol. Energy Mater. Sol. Cells **102**, 173 (2012)
46. M. Fischer, A. Metz, S. Raithel, Semi international technology roadmap for photovoltaics (itrpv)—challenges in c-si technology for suppliers and manufacturers. Proceedings of 27th European photovoltaic solar energy conference, p. 527 (2012)
47. D.M. Powell, M.T. Winkler, H.J. Choi, C.B. Simmons, D.B. Needleman, T. Buonassisi, Energy Environ. Sci. **5**, 5874 (2012)
48. W. Smith, Nature **7**, 303 (1873)
49. W.G. Adams, R.E. Day, Proc. R. Soc. Lond. A **A25**, 113 (1877)
50. A. Mumtaz, G. Amaratunga, Solar energy: photovoltaic electricity generation. *Future Electricity Technologies and Systems* (Cambridge Univesity Press, Cambridge, 2006)
51. C.E. Fritts, Am. J. Sci. **26**, 465 (1883)
52. R.S. Ohl, US Patent 2402662 (1946)
53. M. Wolf, Historical development of solar cells, ed. by C.E. Backus. *Solar Cells* (IEEE Press, Piscatway, 1976)
54. R.A. Sinton, Y. Kwark, J.Y. Gan, R.M. Swanson, IEEE Electron Device Lett. **7**, 567 (1986)
55. IEA photovoltaic power systems programme annual report (2012)
56. M.A. Green, *Silicon Solar Cells: Advanced Principles & Practice* (University of New South Wales, Center for Photovoltaic Devices and Systems, 1995)
57. A. Goetzberger, J. Knobloch, B. Voss, Crystalline Silicon Solar Cells (Willey, New York, 1998)
58. T. Saga, NPG Asia Mater. **2**, 96 (2010)
59. W.E. Spear, P.G. Lecomber, Solid State Commun. **17**, 1193 (1975)
60. D.E. Carlson, C.R. Wronski, Appl. Phys. Lett. **28**, 671 (1976)
61. S. Guha, High-efficiency triple-junction amorphous silicon alloy photovoltaic technology, National Renewable Energy Laboratory, NREL/SR-520-26648 (1999)
62. S. Veprek, V. Marecek, Solid-State Electron. **11**, 683 (1968)
63. M. Yoshimi, T. Sasaki, T. Sawada, T. Suezaki, T. Meguro, T. Matsuda, K. Santo, K. Wadano, M. Ichikawa, A. Nakajima, K. Yamamoto, High efficiency thin film silicon hybrid solar cell module on 1 m2-class large area substrate, in *3rd World Conference on Photovoltaic Energy Conversion* (2003)
64. S.W. Ahn, S.E. Lee, H.M. Lee, Toward commercialization of triple-junction thin-film silicon solar panel with >12% efficiency, in *27th European Photovoltaic Solar Energy Conference* (2012)
65. M. Tanaka, M. Taguchi, T. Matsuyama, T. Sawada, S. Tsuda, S. Nakano, H. Hanafusa, Y. Kuwano, Jpn. J. Appl. Phys. Part 1-Regul. Pap. Short Notes Rev. Pap. **31**, 3518 (1992)
66. S. De Wolf, A. Descoeudres, Z.C. Holman, C. Ballif, Green **2**, 7 (2012)
67. K.S. Ji, H. Syn, J. Choi, H.M. Lee, D. Kim, in *Tech. Digest 21st International Photovoltaic Science and Engineering Conference*, Fukuoka, Japan (2011)
68. N. Mingirulli, J. Haschke, R. Gogolin, R. Ferre, T.F. Schulze, J. Dusterhoft, N.P. Harder, L. Korte, R. Brendel, B. Rech, Physica Status Solidi-RRL **5**, 159 (2011)
69. M. Mews, T.F. Schulze, N. Mingirulli, L. Korte, Appl. Phys. Lett. 102, 122106 (2013)
70. B. Hoex, J. Schmidt, P. Pohl, M.C.M. van de Sanden, W.M.M. Kessels, J. Appl. Phys. **104**, (2008)
71. D.S. Stepanov, N.P. Kherani, Appl. Phys. Lett. **101**, 171602 (2012)

72. Z.R. Chowdhury, K. Cho, N.P. Kherani, Appl. Phys. Lett. **101**, 221110 (2012)
73. E. Kheirandish, *The Arabic Version of Euclid's Optics* (Edited and translated with historical introduction and commentray) (Springer, New York, 1999)
74. J.B. Keller, Bull. Amer. Math. Soc. **84**, 727 (1978)
75. K.B. Wolf, G. Krötzsch, Eur. J. Phys. **16**, 14 (1995)
76. Y.Z. Li, Z.H. Lu, H.W. Yin, X.D. Yu, X.H. Liu, J. Zi, Phys. Rev. E **72**, 010902 (2005)
77. P. Vukusic, J.R. Sambles, Nature **424**, 852 (2003)
78. H.A. Macleod, *Thin-Film Optical Filters* (Institute of Physics Publishing, Bristol, 2001)
79. J.W. Strutt (Lord Rayleigh), Phil. Mag. S. 5, **26**, 256 (1888)
80. Y.A. Vlasov, X.Z. Bo, J.C. Sturm, D.J. Norris, Nature **414**, 289 (2001)
81. A. Blanco, E. Chomski, S. Grabtchak, M. Ibisate, S. John, S.W. Leonard, C. Lopez, F. Meseguer, H. Miguez, J.P. Mondia, G.A. Ozin, O. Toader, H.M. van Driel, Nature **405**, 437 (2000)
82. A.E. St. John, U.S. Patent 3 487 223 (1969)
83. D. Redfield, Appl. Phys. Lett. **25**, 647 (1974)
84. E. Yablonovitch, G.D. Cody, IEEE Trans. Electron Devices **29**, 300 (1982)
85. P. Sheng, A.N. Bloch, R.S. Stepleman, Appl. Phys. Lett. **43**, 579 (1983)
86. G. Demesy, S. John, J. Appl. Phys. **112**, 074326 (2012)
87. E. Yablonovitch, J. Mod. Opt. **41**, 173 (1994)
88. R.D. Meade, K.D. Brommer, A.M. Rappe, J.D. Joannopoulos, Phys. Rev. B **44**, 10961 (1991)
89. K.M. Ho, C.T. Chan, C.M. Soukoulis, Phys. Rev. Lett. **65**, 3152 (1990)
90. B.E. Chomski, S. Johh, C.L. Fernandez, J.F.M. Rico, G.A. Ozin, PCT Application: PCT/CA2001/000049 (2001)
91. L.C. Kimerling, N. Toyoda, W. Kazumi, PCT/US2002/020028 (2002)
92. X. Duan, L.C. Kimerling, Y. Yi, L. Zeng, PCT/US2005/027264 (2005)
93. R.B. Wehrspohn, Applications of silicon-based photonic crystals. Appl. Phys. Lett. **87**, 224106 (2005)
94. M. Peters, J.C. Goldschmidt, P. Loper, B. Gross, J. Upping, F. Dimroth, R.B. Wehrspohn, B. Blasi, Energies **3**, 171 (2010)
95. S.B. Mallick, N.P. Sergeant, M. Agrawal, J.Y. Lee, P. Peumans, MRS Bull. **36**, 453 (2011)
96. L. Zeng, P. Bermel, Y. Yi, B.A. Alamariu, K.A. Broderick, J. Liu, C. Hong, X. Duan, J. Joannopoulos, L.C. Kimerling, Appl. Phys. Lett. **93**, 221105 (2008)
97. A. Chutinan, N.P. Kherani, S. Zukotynski, Opt. Express **17**, 8871 (2009)
98. S.B. Mallick, M. Agrawal, P. Peumans, Opt. Express **18**, 5691 (2010)
99. A. Chutinan, S. John, Phys. Rev. A **78**, 023825 (2008)
100. A. Deinega, S. John, J. Appl. Phys. **112**, 074326 (2012)
101. S.E. Han, G. Chen, Nano Lett. **10**, 4692 (2010)
102. S.K. Karuturi, L.J. Liu, L.T. Su, A. Chutinan, N.P. Kherani, T.K. Chan, T. Osipowicz, A.I.Y. Tok, Nanoscale **3**, 4951 (2011)
103. A. Oskooi, P.A. Favuzzi, Y. Tanaka, H. Shigeta, Y. Kawakami, S. Noda, Appl. Phys. Lett. **100**, 181110 (2012)
104. S. Nishimura, N. Abrams, B.A. Lewis, L.I. Halaoui, T.E. Mallouk, K.D. Benkstein, J. van de Lagemaat, A.J. Frank, J. Am. Chem. Soc. **125**, 6306 (2003)
105. A. Mihi, H. Miguez, J. Phys. Chem. B **109**, 15968 (2005)
106. S.H. Zaidi, J.M. Gee, D.S. Ruby, S.R.J. Brueck, Characterization of si nanostructured surfaces, ed. by A. Lakhtakia, R.F. Messier (eds). Engineered Nanostructural Films and Materials, vol. 3790 (Spie-Int Soc Optical Engineering, Bellingham, 1999), p. 151
107. S.E. Han, G. Chen, Nano Lett. **10**, 1012 (2010)
108. X. Sheng, J.F. Liu, N. Coronel, A.M. Agarwal, J. Michel, L.C. Kimerling, IEEE Photonics Technol. Lett. **22**, 1394 (2010)
109. A. Mavrokefalos, S.E. Han, S. Yerci, M.S. Branham, G. Chen, Nano Lett. **12**, 2792 (2012)
110. K.X.Z. Wang, Z.F. Yu, V. Liu, Y. Cui, S.H. Fan, Nano Lett. **12**, 1616 (2012)
111. K. Kumar, K.K.C. Lee, P.R. Herman, J. Nogami, N.P. Kherani, Appl. Phys. Lett. **101**, 222106 (2012)

112. F. Meillaud, A. Shah, C. Droz, E. Vallat-Sauvain, C. Miazza, Sol. Energy Mater. Sol. Cells **90**, 2952 (2006)
113. T. Soderstrom, F.J. Haug, X. Niquille, V. Terrazzoni, C. Ballif, Appl. Phys. Lett. **94**, 063501 (2009)
114. P. Buehlmann, J. Bailat, D. Domine, A. Billet, F. Meillaud, A. Feltrin, C. Ballif, Appl. Phys. Lett. **91**, 143505 (2007)
115. P.G. O'Brien, A. Chutinan, K. Leong, N.P. Kherani, G.A. Ozin, S. Zukotynski, Opt. Express **18**, 4478 (2010)
116. C. Battaglia, C.M. Hsu, K. Soderstrom, J. Escarre, F.J. Haug, M. Charriere, M. Boccard, M. Despeisse, D.T.L. Alexander, M. Cantoni, Y. Cui, C. Ballif, Acs Nano **6**, 2790 (2012)
117. X. Sheng, S.G. Johnson, L.Z. Broderick, J. Michel, L.C. Kimerling, Appl. Phys. Lett. **100**, 111110 (2012)
118. X. Sheng, S.G. Johnson, J. Michel, L.C. Kimerling, Opt. Express **19**, A841 (2011)
119. Y.H. Kuang, K.H.M. van der Werf, Z.S. Houweling, R.E.I. Schropp, Appl. Phys. Lett. **98**, 151110 (2011)
120. R. Yu, Q. Lin, S.F. Leung, Z. Fan, Nano Energy **1**, 57 (2012)
121. S.Q. Yu, B. Witzigmann, Opt. Express **21**, A167 (2013)
122. P.G. O'Brien, L.-P. Heiniger, N. Soheilnia, Y. Yang, N.P. Kherani, M. Grätzel, G.A. Ozin, N. Tétreault, Adv. Mater. **25**, 5734–5741 (2013)
123. Y. Yang, P.G. O'Brien, G.A. Ozin, N.P. Kherani, Appl. Phys. Lett. **103**, 221109 (2013)
124. R.H. Fan, L.H. Zhu, R.W. Peng, X.R. Huang, D.X. Qi, X.P. Ren, Q. Hu, M. Wang, Phys. Rev. B **87**, 195444 (2013)
125. C. Wang, S.C. Yu, W. Chen, C. Sun, Sci. Rep. **3**, 3513 (2013)
126. M.D. Vece, Y. Kuang, J.K. Rath, L. van Dijk, R.E.I. Schropp, Rep. Prog. Phys. **76**, 106502 (2013)

http://www.springer.com/978-981-287-130-5

Excitonic and Photonic Processes in Materials
Singh, J.; Williams, R.T. (Eds.)
2015, XVI, 358 p. 184 illus., 113 illus. in color.,
Hardcover
ISBN: 978-981-287-130-5